Water Resources Management

# Evapotranspiration from an olive orchard using remote sensing-based dual crop coefficient approach

--Manuscript Draft--

| | |
|---|---|
| **Manuscript Number:** | WARM-D-13-00088R1 |
| **Full Title:** | Evapotranspiration from an olive orchard using remote sensing-based dual crop coefficient approach |
| **Article Type:** | General paper |
| **Keywords:** | plant transpiration, optical remote sensing; dual crop coefficient. |
| **Corresponding Author:** | Carmelo Cammalleri<br><br>UNITED STATES |
| **Corresponding Author Secondary Information:** | |
| **Corresponding Author's Institution:** | |
| **Corresponding Author's Secondary Institution:** | |
| **First Author:** | Carmelo Cammalleri |
| **First Author Secondary Information:** | |
| **Order of Authors:** | Carmelo Cammalleri |
| | Giuseppe Ciraolo |
| | Mario Minacapilli |
| | Giovanni Rallo |
| **Order of Authors Secondary Information:** | |
| **Abstract:** | A remote sensing-based approach to estimate actual evapotranspiration (ET) was tested in an area covered by olive trees and characterized by Mediterranean climate. The methodology is a modified version of the standard FAO-56 dual crop coefficient procedure, in which the crop potential transpiration, Tp, is obtained by directly applying the Penman-Monteith (PM) equation with actual canopy characteristics (i.e., leaf area index, albedo and canopy height) derived from optical remote sensing data. Due to the minimum requirement of in-situ ancillary inputs, the methodology is suitable also for applications on large areas where the use of tabled crop coefficient values become problematic, due to the need of corrections for specific crop parameters, i.e., percentage of ground cover, crop height, phenological cycles, etc.. The methodology was applied using seven airborne remote sensing images acquired during spring-autumn 2008. The estimates based on PM approach always outperforms the ones obtained using simple crop coefficient constant values. Additionally, the comparison of simulated daily evapotranspiration and transpiration with the values observed by eddy correlation and sap flow techniques, respectively, shows a substantial agreement during both dry and wet days with an accuracy in the order of 0.5 and 0.3 mm/d, respectively. The obtained results suggest the capability of the proposed approach to correctly partition evaporation and transpiration components during both the irrigation season and rainy period also under conditions of significant reduction of actual ET from the potential one. |

# Evapotranspiration from an olive orchard using remote sensing-based dual crop coefficient approach

C. Cammalleri[1,*], G. Ciraolo[1], M. Minacapilli[2], G. Rallo[2]

{1} Department of Civil, Environmental, Aerospace, Materials Engineering (DICAM), Università degli Studi di Palermo, Italy.

{2} Department of AgroForestry Sciences (SAF), Università degli Studi di Palermo, Italy.

{*} Now at: U.S. Department of Agricultural, Agricultural Research Service - Hydrology and Remote Sensing Laboratory.

**Corresponding author:**

Carmelo Cammalleri, PhD.

U.S. Department of Agricultural, Agricultural Research Service

Hydrology and Remote Sensing Laboratory.

10300 Baltimore Ave. Bldg. 007 BARC-West.

Beltsville, MD 20705-2350.

e-mail: cammillino@gmail.com.

Tel: (301)-504-5420.

Fax: (301)-504-8931.

## ABSTRACT

A remote sensing-based approach to estimate actual evapotranspiration (*ET*) was tested in an area covered by olive trees and characterized by Mediterranean climate. The methodology is a modified version of the standard FAO-56 dual crop coefficient procedure, in which the crop potential transpiration, $T_{p,}$ is obtained by directly applying the Penman-Monteith (PM) equation with actual canopy characteristics (*i.e.*, leaf area index, albedo and canopy height) derived from optical remote sensing data. Due to the minimum requirement of *in-situ* ancillary inputs, the methodology is suitable also for applications on large areas where the use of tabled crop coefficient values become problematic, due to the need of corrections for specific crop parameters, *i.e.*, percentage of ground cover, crop height, phenological cycles, etc.. The methodology was applied using seven airborne remote sensing images acquired during spring-autumn 2008. The estimates based on PM approach always outperforms the ones obtained using simple crop coefficient constant values. Additionally, the comparison of simulated daily evapotranspiration and transpiration with the values observed by eddy correlation and sap flow techniques, respectively, shows a substantial agreement during both dry and wet days with an accuracy in the order of 0.5 and 0.3 mm $d^{-1}$, respectively. The obtained results suggest the capability of the proposed approach to correctly partition evaporation and transpiration components during both the irrigation season and rainy period also under conditions of significant reduction of actual *ET* from the potential one.



**Keywords:** plant transpiration, optical remote sensing; dual crop coefficient.

## 1. INTRODUCTION

In Mediterranean regions, where the growing season is generally hot and dry, an accurate estimation of crop water requirement is desirable for optimizing water resource usage. In particular, a reliable estimate of daily evapotranspiration (*ET*) fluxes in such environments is one of the main issues in agro-hydrological community, and it is assumed as a key step to challenge the increasing reduction in water availability. Additionally, in sparse cropped system (*i.e.*, olive trees, vineyards), the capability to partition *ET* into soil evaporation ($E_s$) and crop transpiration ($T_c$) is further relevant because only the latter is effectively related to the crop water stress, hence to crop productivity.

In the common agro-hydrological applications, estimations of *ET* are realized separating the effects of: (i) atmospheric demand, via reference evapotranspiration ($ET_0$), (ii) crop characteristics, using crop coefficient, and (iii) water stress, by means of reduction factors, as suggested in the standardized FAO-56 procedure (Allen et al. 1998). This approach has some limitations in its applicability over large areas due to the possible discrepancy between actual crop characteristics (percentage of ground, cover, crop height, phenological stage, etc.) and the values used to derive tabled crop coefficients, and the difficulty to acquire all these information for the correction of the standard values.

Some authors (*e.g.*, Allen and Pereira 2009) have highlighted the need of correcting the FAO-56 tabled values to take into account the actual local crop characteristics (*i.e.*, height, ground coverage), which can be quite different from the 'standard' values due to the large variability of such characteristics within the same crop type. This issue is particularly relevant for orchards

(*i.e.*, olive grove), natural vegetation and rural landscapes, where vegetation amount, height, and density are highly variable (Allen and Pereira 2009). Additionally, crop coefficients values have to be corrected for climate effects in the case of tall vegetation, because differences in roughness cause discrepancies under high wind speed conditions (Doorenbos and Pruitt 1975). Such corrections are generally negligible for most crops, especially if alfalfa reference is used (Pereira et al. 1999; Wright 1982), but they become relevant for sparse trees.

Methodologies proposed in the literature to correct tabled crop coefficients for both actual crop characteristics and climatic effects are generally based on the knowledge of site-specific parameters, which can be easily retrieved for local scale applications; however, the use of such relationships for large areas is problematic due to the obvious lack of field-scale information. The increasing availability of remote observations in the last decades fed the development of a number of methodologies to enlarge the applicability of crop coefficients based estimation on large areas. In fact, some authors (*e.g.*, Bausch et al. 1987; Heilman et al. 1982) have highlighted the strong connection between crop coefficients and canopy reflectance at different scales. These considerations were used to implement either empirical relationships between vegetation indices and crop coefficients, as the ones introduced by González-Dugo and Mateos (2008), or physical based relationships between crop characteristics (albedo, leaf area index, plant height) and crop coefficients (D'Urso and Menenti 1995; Minacapilli et al. 2008) or potential $ET$ ($T_p$).

The use of remote estimation of crop coefficients, can be seen as an alternative to the widely adopted residual surface energy balance (SEB) approaches, which are intensively applied on sparse crops in different regions in the past years (*e.g.*, Abid Karray et al. 2008; Er-Raki et al. 2010; Minacapilli et al. 2009). In fact, despite the appeal of residual SEB, its practical

applicability for weekly, monthly and seasonal scales estimates generally suffers of a lack of high spatiotemporal resolution thermal data, which are the key input of SEBs as proxy water stress (Kalma et al. 2008). On the basis of this consideration, the use of an hydrological model to detect water stress can be seen as a suitable alternative in areas characterized by high spatial fragmentation, where a sufficiently high spatial resolution of the thermal data is not operationally available at this time.

This paper tests the reliability of a methodology based on the use of remote estimations of potential crop transpiration into the FAO-56 dual crop coefficient modeling framework for the continuous assessment of daily *ET* in areas characterized by sparse crops. In particular, the application of this methodology is realized on an irrigated olive grove in a typical Mediterranean climate by means of seven high resolution airborne images acquired during June-October 2008. The main features of the model to be evaluated in such environment are: i) the reliability of remotely-assessed potential crop transpiration for olive crops, and ii) the capability of FAO-56 procedure to capture the dynamic of water stress trough a simple computation of soil water content.

The analysis of model performance is carried out both in terms of daily *ET* and $T_c$ estimates at field scale by means of a joined use of micro-meteorological and sap flow measurements. These observations allow not only to analyze the capability to correctly detect water stress in such dry environment, but also to evaluate the capability of the proposed approach to separate soil and canopy contributes to total *ET* in both dry and wet periods.

## 2. MATERIALS AND METHOD

### 2.1 Model description

In agro-hydrological applications the assessment of daily actual evapotranspiration, $ET$ (mm $d^{-1}$), in sparse system is commonly performed by means of the so-called dual crop coefficient approach (Allen et al. 1998):

$$ET = K_s T_p + K_e ET_0 \quad (1)$$

where $T_p$ and $ET_0$ (mm $d^{-1}$) are crop-potential transpiration and reference evapotranspiration, respectively, $K_s$ is the crop water stress coefficient and $K_e$ is the soil evaporation reduction coefficient. Adopting this definition for $ET$, the second hand first term represents the actual crop transpiration, $T_c$, whereas the second term is the soil evaporation, $E_s$.

In the standard dual crop coefficient FAO-56 procedure, $T_p$ is generally computed by multiplying $ET_0$ and tabled basal crop coefficients (hereafter refer to as $K_c$) which are in general dependent on crop type and development stage ($T_{p\text{-FAO}} = K_c\ ET_0$). FAO-56 procedure also suggest corrections of tabled $K_c$ to reproduce divergence of table values for high wind speed conditions if actual canopy height is known (Allen et al. 1998). Moreover, Allen and Pereira (2009) suggested a procedure to correct tabled values when local detailed information on ground cover are available.

#### *2.1.1 Potential transpiration assessment*

Potential canopy transpiration, $T_p$, is commonly defined as the transpiration of a generic crop in condition of unlimited water availability (Doorenbos and Pruitt 1975). This definition allows

analyzing the effects of water stress as a reduction of the effective value starting from the potential condition. Due to its definition, $T_p$ can be directly related to meteorological variables and crop characteristics only, representing a fundamental upper boundary for the hydrological and surface energy balance models.

The potential transpiration can be generically defined following the approach originally proposed for a single leaf by Penman (1956) and adapted for crop by Monteith (1965), from here on referred to as PM. This approach schematizes the crop as a single big-leaf, allowing $T_{p\text{-PM}}$ computation by means of equation:

$$T_{p\text{-PM}} = \frac{1}{\lambda} \frac{\Delta\left(R_{n,\text{sw}} - R_{n,\text{lw}} - G_0\right) + \rho c_p \dfrac{\left(e_s - e_a\right)}{r_{ah}}}{\Delta + \gamma\left(1 + \dfrac{r_{c,\min}}{r_{ah}}\right)} \quad (2)$$

where $\lambda$ represents the latent heat of vaporization ($\approx$ 2.45 MJ kg$^{-1}$), $\rho$ is the mean air density (kg m$^{-3}$), $c_p$ is the specific heat of the air at constant pressure (J kg$^{-1}$ K$^{-1}$), and the others terms are defined as follow.

The term $R_{n,\text{sw}}$ represents the short-wave net radiation (MJ m$^{-2}$ d$^{-1}$) computable as:

$$R_{n,\text{sw}} = (1-\alpha)R_s \quad (3)$$

where $R_s$ is the incoming solar radiation (MJ m$^{-2}$ d$^{-1}$) and $\alpha$ is the surface albedo. Long-wave net radiation, $R_{n,\text{lw}}$ (MJ m$^{-2}$ d$^{-1}$) is generally computed by means of the well-known simplified approach introduced in the FAO-56 paper that takes into account the strong relationship between air surface temperature and the absolute vegetation temperature for well watered crops (Allen et

al. 1998). The soil heat flux, $G_0$ (MJ m$^{-2}$ d$^{-1}$), is computed by means of simplified relationship as a constant fraction of the total net radiation ($R_{n,\mathrm{sw}} + R_{n,\mathrm{lw}}$).

The term $r_{c,\min}$ is the crop stomatal resistance (s m$^{-1}$) in absence of stress condition, hence when stomata oppose the minimum resistance to water loss. This value can be computed as suggested by Allen et al. (1989):

$$r_{c,\min} = \frac{r_{\mathrm{leaf}}}{0.5\mathrm{LAI}} \tag{4}$$

where LAI is the leaf area index (m$^2$ m$^{-2}$) and $r_{\mathrm{leaf}}$ represent the single leaf stomatal resistance (Sellers et al. 1992) assumed equal to 100 s m$^{-1}$. This value, suggested in the literature for alfalfa and grass canopies was successfully used in more physically based approaches over similar study cases (Minacapilli et al. 2009; Cammalleri and Ciraolo 2012), likely thanks to the small contribution of stem and braches resistances to the bulk value under non-stress conditions.

The aerodynamic resistance, $r_{ah}$ (s m$^{-1}$), represents the resistance of the atmosphere to the heat and water vapor transfer, and can be modeled as (Brutsaert 1982):

$$r_{ah} = \frac{\ln\left(\frac{z_u - 0.667h_c}{0.123h_c}\right)\ln\left(\frac{z_T - 0.667h_c}{0.0123h_c}\right)}{0.168U_z} \tag{5}$$

where $h_c$ (m) is the canopy height, $z_u$ and $z_T$ (m) represent the measurements height of wind velocity and air temperature, respectively. Correction factors for non-neutral atmospheric conditions are relatively small even for sparse vegetation under dry conditions if $z_u$ and $z_T$ are close enough to the surface.

The reference transpiration, $ET_0$, used in FAO-56 can be derived from Eq. (2) by introducing the proprieties of a "*hypothetical grass reference crop with an assumed crop height of 0.12 m, a fixed surface resistance of 70 s* $m^{-1}$ *and an albedo of 0.23*". Instead, the direct application of Eq. (2) with crop-specific values of LAI, $\alpha$ and $h_c$ in Eqs. (3)-(5) allows deriving the $T_p$ of any crop (again, under the assumption of a known constant $r_{leaf}$ value). Recently, several authors (*e.g.*, Choudhury et al. 1994; D'Urso and Menenti 1995) have suggested to derive these crop-specific variables from remote sensing data, in order to apply the PM in a spatial distributed way. This approach allows us to directly take into account the spatial distribution of the effective crop conditions (by means of $\alpha$, $h_c$ and LAI), supplying for the need of both tabled crop coefficients and local corrections.

### *2.1.2 Estimation of water stress coefficients*

In the FAO-56 procedure, root zone depletion is used to account for water stress at daily basis using a simple tipping bucket water balance approach:

$$D_i = D_{i-1} - P_i - I_i + ET_i + DP_i \quad (6)$$

where $D_i$ and $D_{i-1}$ are the root zone depletions at the end of day $i$ and $i-1$, respectively, $P_i$ is the net precipitation, $I_i$ is the irrigation supply, $ET_i$ is the actual evapotranspiration and $DP_i$ is the deep percolation of water moving out of the root zone. All the terms are expressed in (mm $d^{-1}$).

The domain of $D_i$ is between 0, which occurs when the soil water content is at the field capacity, $\theta_{fc}$, and a maximum value, corresponding to the total available water, *TAW* (mm), for the plant, given by the following equation:

$$TAW = 1000\left(\theta_{fc} - \theta_{wp}\right)_i Z_r \quad (7)$$

where $\theta_{wp}$ ($m^3$ $m^{-3}$) is the soil water content at wilting point and $Z_r$ (m) the depth of the root system.

The plat transpiration reduction factor, $K_s$, variable between 0 and 1, can be express as:

$$K_s = \frac{TAW - D_i}{TAW - RAW} \quad (8)$$

where $RAW$ (mm) is the readily available water, that can be obtained multiplying $TAW$ to a depletion coefficient, $p$, taking into account the crop water stress resistance. Van Diepen et al. (1988) proposed a simple empirical function for adjusting $p$ for different conditions of atmospheric evaporative demand.

The soil evaporation coefficient, $K_e$, is generally considered proportional to the amount of water in the soil top layer, or:

$$K_e = \min\left[ K_r \left( K_{c,\max} - K_c \right), \quad f_{ew} K_{c,\max} \right] \quad (9)$$

where $K_r$ is a dimensionless evaporation reduction coefficient, depending on the cumulative depth of water evaporated from the topsoil, $f_{ew}$ is the fraction of the soil that is both exposed and wetted, *i.e.*, the fraction of soil surface from which most evaporation occurs, and $K_{c,\max}$ is the upper limit for the evaporation and transpiration from any cropped surface, assumed equal to a fixed value of 1.3. The reduction of actual evaporation when the amount of water in the surface soil layer decreases is accounted as:

$$K_r = \frac{TEW - D_{e,i}}{TEW - REW} \quad (10)$$

where *REW* (mm) is the readily evaporable water, *TEW* is the maximum cumulative depth of evaporation from the soil surface layer ($Z_e$ = 0.1 m) and $D_{e,i}$ (mm) is cumulative depletion at the end of i-th day.

## 2.2 Experimental site and measurements

### *2.2.1 Study area description*

The study area (Fig. 1) is located in south-west part of Sicily (Italy) near Castelvetrano (TP) town, in correspondence of the "Rocchetta" olive farm (Lat: 37º 38' 35" N; Lon: 12º 50' 50'' E). In particular, the experimental area is an olive field of about 13 ha, demarcated in Fig. 1, almost totally covered by cv. "*Nocellara del Belice*" olive trees, planted with a regular grid of about 8 × 5 $m^2$ (~ 250 trees/ha).

The soil can be classified as silty clay loam, following the USDA classification, with mean clay, silt and sand contents of about 24, 16 and 60%, respectively. The study site was irrigated by drop-by-drop system, with a nominal capacity of a single dripper of 8 liters per hour, and a field-average irrigation water flow of about 4 mm $h^{-1}$ (with 4 drippers per tree and assuming a fraction of soil wetted by irrigation, $f_w$, of 0.2). The area is characterized by a typical Mediterranean climate, with moderate rainfall during autumn and winter periods and high air temperature and scarce precipitation during summer.

### *2.2.2 Surface fluxes and standard meteorological measurements*

The standard meteorological variables required for both $ET_0$ and $T_p$ computation were provided by the SIAS (Servizio Informativo Agrometeorologico Siciliano) weather station n. 302, located

at about 200 m north-east from the experimental field (see Fig. 1). The station is equipped with sensors for the measurement of the following meteorological variables: air temperature at 2 m, precipitation, relative humidity, wind speed and direction at 2 and 10 m, air pressure, global incoming solar radiation. All the data are available on the SIAS website (http://www.sias.regione.sicilia.it/) at different temporal scale (hourly, daily, and monthly); in order to apply the FAO-56 approach in this study, hourly data have been used.

Surface energy fluxes in the olive orchard were continuously monitored during the entire study period by means of 2 micro-meteorological installations: a small aperture scintillometer and an eddy covariance tower. The scintillometer (SAS) system included a displaced beam small aperture scintillometer (SLS20, Scintec AG - Germany), a two component (total incoming and outgoing) pyrradiometer (model 8111, Schenk GmbH - Germany), and three soil heat plates (HFP01SC, Hukseflux - The Netherlands). The SAS was installed at a height of 7 m above the ground (agl), with a path length of about 95 m; the pyrradiometer was installed in correspondence of SAS transmitter an elevation of 8 m a.g.l., and the three flux plates were set beneath the canopy foliage, in an exposed bare soil area and in an intermediate location, at depth of about 0.10 m below the ground. Due to the preparation of the soil by ploughing, the heat storage above the plates has been neglected. Data from the three soil plates have been averaged to estimate field-scale representative values. This installation allowed the direct measurements of net radiation and soil heat flux, indirect measurements of sensible heat flux via the Monin-Obukhov surface layer similarity theory (Hartogensis 2006; Thiermann and Grassl 1992), and then the derivation of latent heat flux as a residual term of the surface energy balance.

The eddy covariance system (EC) was located in the northern part of the olive field, and it is part of the CarboItaly network. The instruments include a three-dimension sonic anemometer (CSAT3-3D, Campbell Scientific Inc. - Logan, UT, USA) and an open-path gas analyzer (LI7500, Li-Cor Biosciences Inc. - Lincoln, NE, USA) installed at an elevation of 8 m agl, a 2-component net radiometer (NR-Lite-L, Kipp & Zonen - The Netherlands), and two HFP01SC flux plates. This installation measured all the terms of the surface energy balance. It is well known that in most cases turbulent fluxes measured by the eddy covariance technique suffer from lack of energy balance closure due to a number of factors (Allen et al. 2011). In this experiment, the balance closure was satisfactory, with a closure ratio of approximately 0.87, and a long term multi-instrument intercomparison detected in the latent heat flux observations the main source of error. Considering that PM formulation relies on a perfect surface energy balance closure, EC flux closure was enforced by assigning energy residuals to the latent heat flux. For validation purpose, flux observations from the two installations were averaged and assumed to be representative of the field average (see Cammalleri et al. 2010).

Additionally, trees transpiration was monitored on three plants by using thermal dissipation probes (TDP, Fig. 1) and applying the method of Granier (1987). In particular, sap velocity was measured every 30-min using the heat dissipation technique. The temperature difference between the heated upper needle and the un-heated lower needle during the day, combined with the temperature difference at night (obtained on the basis of a regression between minimum values recorded in 10 days and the time) allows estimating the tree sap flow by multiply sap velocity with the active cross section area. The daily stand transpiration fluxes were then obtained by scaling up the plant scale values taking into account the pertinence area of a single plant (40 $m^2$) and the ratio between plot average LAI and single plant one (Cammalleri et al. 2012). The up-

scaling factor for each plant was derived using the remotely sensed LAI maps described in the next section.

### *2.2.3 Remote sensing data acquisition and processing*

During the summer-autumn 2008 the test site was interested by the acquisition of 7 high resolution multispectral images. The airborne remote sensing data acquisitions were realized by "Terrasystem s.r.l." with a *SKY ARROW 650 TC/TCNS* aircraft, at a high of about 1000 m agl. The platform has on board a multi-spectral camera (MS4100, Duncantech Inc. – Auburn, CA, USA) with 3 spectral bands at green (G, 530-570 nm), red (R, 650-690 nm) and near infrared (NIR, 767-832 nm) wavelengths, and a thermal camera (SC500/A40M, FLIR System Inc. – Wilsonville, OR, USA) with a broad band in the range 7.5-13 μm. The nominal spatial resolution was of about 0.6 m for VIS/NIR acquisition, and 1.7 m for thermal-IR data. In Table 1 are reported the acquisition dates, with indication of the mean overpass times.

Additionally, during the imagery acquisitions, the test site was interested by a set of in-field measurements for radiometric and bio-physic characterization. Specifically, spectroradiometric measurements were collected with a portable spectroradiometer (FieldSpec HandHeld, ASD Inc. – Boulder, CO, USA) over a number of natural and artificial surfaces with different radiometric characteristics, and LAI was measured for different crops using an optical not-destructive instrument (LAI2000, Biosciences Inc. - Lincoln, NE, USA) together with canopy height measurements.

The raw dataset (G, R and NIR bands) was spatial averaged to a resolution of 12 m in order to simulate the spatial resolution of the nowadays available satellite data (*e.g.*, ASTER, SPOT, FORMOSAT-2, RapidEye). The dataset constituted by the 7 acquisitions has been radiometrically calibrated, and the atmospheric influence was removed by means of the empirical line method (Slater et al. 1996) using the spectroradiometric *in-situ* measurements. The calibrated bands were used to derive the Normalized Difference Vegetation Index, NDVI, (Rouse et al. 1973). Successively, a semi-empirical relationship NDVI-LAI based on the approach proposed by Clevers (1989) was calibrated using the ordinary least-squares method on the *in-situ* LAI and NDVI measurements. A single calibrated relationship was used in order to assess the LAI maps for the different dates. Canopy heights have been retrieved by means of local calibrated LAI-based polynomial empirical relationship, as suggested by Anderson et al. (2004). Finally, surface albedo maps were obtained by means of a linear combination of the remotely-observed spectral reflectances (Price 1990). The weighting factors of this relationship were calibrated for the given sensor by means of the ordinary least-squares method directly applied on the *in-situ* observed data. Specifically, the sensor spectral response for each band was used on the *in-situ* spectra in order to simulate the remotely-observed reflectance for each target, whereas the corresponding *in-situ* surface albedo was derived from the spectral integration of the observed signatures in the whole short-wave range. Examples of the accuracy of these calibrations are reported in Fig. 2 relatively to the first acquisition date.

Figure 3 shows an example of albedo (upper left panel), NDVI (upper right panel), LAI (lower left panel) and canopy height (lower right panel) maps retrieved in correspondence of the second acquisition day (DOY 185).

## 3. RESULTS AND DISCUSSION

### 3.1 Analysis of potential transpiration

The remotely sensed maps of albedo, LAI and canopy height, and the locally observed meteorological variables, were used to derive daily $T_p$ during the 2008 irrigation season (from June to October). Particularly, hourly estimations were made using hourly meteorological data; afterwards, daily estimates were obtained by means of temporal integration.

In order to obtain a benchmark $T_p$ estimation, $ET_0$ was assessed at hourly basis using the same meteorological dataset, and tabled $K_c$ was used to derive potential values. This case corresponds to the common practice to derive $K_c$ values from a land use map and tabled FAO-56 values. In particular, FAO-56 tabled $K_c$ for olive crop during mid phenological stage can be assumed equal to a constant value of 0.65. The effect of this value on actual *ET* will be discussed successively.

The remote $T_{p\text{-PM}}$ estimates obtained during the study period are compared in Fig. 4 with the ones obtained from FAO-56 tabled $K_c$. This scatterplot shows a systematic bias between the two estimates, and it also highlights an evident scatter. This analysis suggests a significant difference between the PM-derived $K_c$ derived and the tabled ones, with a Mean Absolute Difference (MAD) in the order of 1.0 mm $d^{-1}$, and a linear regression line that differs significantly from the perfect matching (slope = 0.6 and intercept = 0.6 mm $d^{-1}$). These results seem to suggest that a local correction of table $K_c$ is likely required for this study site, probably due to a canopy coverage lower than the one assumed in FAO-56 for 'standard' olive (40 to 60%). This hypothesis is further tested in the next section in terms of modeled actual *ET*.

### 3.2 Validation of daily ET and $T_c$ estimations

The $T_{p\text{-PM}}$ maps and the $ET_0$ time series were used as inputs of the FAO-56 hydrological model, as well as with daily rainfall and irrigation records. The FAO-56 hydrological model was applied in a simulation period of 153 days, from 1 June 2008 (DOY 163) to the end of October (DOY 305); during this period 4 irrigations of 12 hours were provided (DOY 195, 225-227) during nighttime. The main soil hydrological parameters were derived from *in-situ* observations, as summarized in Table 2.

Additionally, as discussed in the previous section, the impact of locally calibrated constant $K_c$ on simulated daily *ET* was evaluated by means of a set of different values within a reliable range for the specific crop type ($0.4 - 0.8$). These values cover the whole range of variability for $K_c$ in olive trees reported in the literature from low density to extensively planted. The 'optimal' $K_c$ for this site is then selected as the one characterized by minimum error in reproducing observed *ET* data. This analysis aims at evaluate the classical FAO-56 model performance when the crop type is known, but no local information are available, as in the case of crop coefficient derived from a land use map. In this case the uncertainty in $K_c$ can be associated to the typical range of variability of $K_c$ for the specific crop type.

Figure 5 compares the mean absolute difference (MAD, panel a) and the root mean square difference (RMSD, panel b) values obtained on actual *ET* using different $K_c$ values by comparison with micro-meteorological observations. Additionally, horizontal dotted line represent the value obtained using PM formulation as input of FAO-56 hydrological model.

These plots highlight how PM models is characterized by the lowest error, in terms of both MAD and RMSD. Also, it is possible to notice how the 'optimal' constant $K_c$ for this site can be assumed equal to 0.5, which is lower than the tabled one (0.65) and in between the values reported by Allen and Pereira (2009) for low (25% coverage) and med (50% coverage) density. This result is not surprising, considering that FAO-56 tabled value corresponds to a ground coverage of 40-60%, whereas the actual vegetation coverage is about 35%. Additionally, these results are in agreement with the ones reported in Fig. 4, where the use of tabled $K_c$ causes a systematic overestimation of PM values.

The difference between the performance of PM-based estimates and 'optimal' constant $K_c$ can be associated to the effects of daily fluctuation of $K_c$ due to change in daily meteorological conditions. These effects are intrinsically accounted in PM-based approach which directly use Eq. (2), while them should be explicitly introduced to tabled value as discussed in FAO-56 paper as well as in Allen and Pereira (2009). However, assuming again as a benchmark the estimation obtained from a land use map, these correction cannot be applied without further local information. The estimates obtained by using an 'optimal' $K_c$ (site specific as a function of ground coverage) and introducing the effect of meteorological conditions through field-average LAI and $h_c$ (derived from remote observations) are almost identical to PM-based ones (not reported here); however, no advantages are related to the use of this approach (tabled $K_c$ + local correction for ground coverage, LAI and $h_c$) compared to the direct application of the PM formulation in terms of required inputs, especially on large areas where these data have to be derived from remote sensing.

On the basis of the results reported in Fig. 5, the daily *ET* obtained from the simulation using PM estimates of $T_p$, Eq. (2), is depicted in Fig. 6, together with the *ET* observed values and the hydrological inputs (rainfall and irrigation). The comparison between modeled and observed signals further highlights the good correspondence in the magnitude of *ET* across the whole simulation period, with a slight underestimation performed by the model during the final days of the simulation period (DOY 275-300).

In addition, the model shows a good capability to reproduce *ET* observations during both the first dry stage (DOY 153-190), when unfortunately only few measurements are available, and irrigation period (DOY 190-250). Moreover, it is possible to notice that the observed increase in *ET* fluxes as a consequence of the rainy days occurred in the late September (DOY 260-270) is well captured by the model. The previously highlighted underestimation after this rainy period can be probably ascribed to fluxes generated by short grasses grown beneath the trees (cover crop), which are not taken into account by the model. This cover crop is evident in the original high-resolution data (0.6 m) in the last 2 acquisition dates, and it responds to change in water availability much faster than olive trees, and it is characterized by different aerodynamic structure and root depth as well.

The general agreement between observations and simulations is achieved by the good correspondence between observed (2.05 mm $d^{-1}$) and modeled (2.01 mm $d^{-1}$) season-average *ET* values during the entire study period. Moreover, the obtained MAD value, equal to 0.48 mm $d^{-1}$, is aligned with the measurement uncertainties for this study site (see Cammalleri et al. 2010), as well as the typical uncertainties of the measurement techniques (Allen et al. 2011). The model performance is comparable with the ones obtained by more detailed modeling schemes

(Cammalleri and Ciraolo 2012; Crow et al. 2008; Er-Raki et al. 2010; Falge et al. 2005; González-Dugo et al. 2009, Mateos et al. 2012; Santos et al. 2012).

Similarly, the analysis of transpirative fluxes, reported in Fig. 7, highlights the good reliability of modeled fluxes during the whole simulation. In particular, it is possible to observe a slightly variability in both observed and modeled values, emphasizing the ability of olive trees to module their response to atmospheric demand also under severe water stress conditions. The comparison between modeled $T_c$ fluxes and sap flow observations shows a substantial agreement, with a slightly decreasing trend in both data probably due to a combined effect of reduction in atmospheric demand and increase in water stress. A good agreement is also achieved during the deficit irrigation phase, despite the large difference between $T_c$ and $T_p$ (see Fig. 7), suggesting the capability of the model to correctly reconstruct $T_c$ fluxes also during significant water stress conditions. The agreement between modeled and observed fluxes can be quantified by a MAD of 0.29 mm $d^{-1}$. The error in $T_c$ estimation seems to be lower than the one for *ET*, and in agreement with the one obtained from the analysis of $T_p$. The relative errors in $T_c$ and *ET* fluxes are rather similar (≈ 20%), and them can be considered satisfactory for operational purposes.

The analysis of the periods DOY 220-250 and DOY 250-300, separately, highlights the good capability of the approach to model transpiration components during both the dry season (when $E_s \approx 0$) and the wet rainy period ($E_s > 0$). The combined examination of $T_c$ and *ET* observations highlights how the soil evaporation contributes are generally negligible during the irrigation days due to the adopted dripped irrigation system characterized by a small wetted surface and nighttime working hours; instead, the soil evaporation is predominant after rainy days due to the high fraction of exposed soil (around 65%). Both these behaviors are well represented by the

model thanks to the dual-crop coefficient approach which allows us to correctly separate the water dynamic in surface layer and root zone.

### 3.3 Analysis of water stress

The performance of the model should be analyzed also in terms of the capability to correctly quantify plant water stress, which is a key factor for managing deficit irrigation. Previous studies (e.g., Rallo and Provenzano, 2013) detected the arise of crop stress at soil matric potential of about –40 m. This value corresponds to a ratio $T_c/ET_0$ of approximately 0.5, which is generally assumed by the farmer as a condition of moderate stress. The secondary panel in both Figs. 6 and 7 shows the normalized values of $ET$ and $T_c$ (via $ET_0$), respectively, in order to provide a proxy of the actual water stress conditions. These figures suggest how similar values of both ratios are observable during the irrigation phase, in the order of 0.25-0.30. The analogies between $ET/ET_0$ and $T_c/ET_0$ series is once more justified by the negligible soil evaporation due to the fast draining of surface soil.

The amount of water supplied thorough irrigation, despite limited, seems to avoid further reduction of the ratio $T_c/ET_0$, which is rather constant during the whole irrigation period. The values assumed by this ratio, always between 0.2 and 0.4, suggest that a high degree of stress is reached in the study area since it is always lower than the threshold 0.5. However, a certain degree of stress is generally required by the farmer in order to maintain a high quality of the final product; from this point of view a ratio $T_c/ET_0 < 0.5$ seems to reach that goal. As previously highlighted, olive trees showed a good capability to module the response to atmospheric demand ($ET_0$); in particular, the average $T_c$ value of about 1.8 mm $d^{-1}$ during the irrigation phase

corresponds to a normalized value (through $ET_0$) of about 0.25, instead the corresponding average values in September is 0.35 (see secondary panel in Fig. 7).

Finally, a further analysis of the evolution of water stress during the study period was performed through the cumulated values of both *ET* and $T_c$. In fact, the occurrence of water stress has to be studied as a dynamic process that is influenced by the prior conditions and not only by the actual one. With this aim, the plots in Fig. 8 report the observed (black line) and modeled (cyan line) *ET* (left panel) and $T_c$ (right panel) cumulative values during the simulation period when observations were available.

The analysis of these cumulative *ET* and $T_c$ data highlights the quite good matching between observed and modeled values, which confirms the suitability of the methodology also in terms of dynamic detecting of crop water stress. Moreover, the intercomparison of season totals (*ET* = 185 mm and $T_c$ = 75 mm) highlights the substantial reduction of actual values from both the atmospheric demand and crop potential condition ($ET_0$ = 465 mm and $T_p$ = 165 mm). These values were computed considering only the days when *ET* and $T_c$ actual observations were available, respectively. On the full simulation period, the total actual *ET* (315 mm) satisfies only ≈ 40% of the atmospheric demand (815 mm), and it is constituted for the 86% by crop transpiration (265 mm). These data result in a season-average crop stress coefficient ($T_c/T_p$) of about 0.5 and a season-average $T_c/ET_0 \approx 0.32$ (lower than the starting-stress threshold of 0.5), which further legitimates the suitability of the model to fairly detect the magnitude of *ET* and $T_c$ fluxes under a notable degree of water stress conditions.

## 4. SUMMARY AND CONCLUSIONS

Crop daily evapotranspiration and transpiration estimates were compared with flux observations made over an olive orchard located in a typical Mediterranean environment. The adopted model requires optical remote sensing data (in visible and near-infrared regions) to assess crop effective characteristics (albedo, LAI and canopy height) and ancillary standard meteorological inputs. The application of PM formula provides direct spatially distributed estimations of potential transpiration, to be introduced in the FAO-56 hydrological balance. This method overcomes the limitations of residual energy balance model related to the lack of thermal data at high spatial/temporal resolution. However, reliable rainfall and irrigation inputs must be available over the region under investigation in order to properly resolve the hydrological balance; additionally, a reliable value for the minimum stomatal resistance (in absence of water stress) have to be assumed for the specific crop type, which can be problematic for particular vegetation types or climatic regions.

The analysis of potential transpiration assessed by the PM approach highlights the better performance compared to simple tabled FAO-56 one. These results confirm the need of local information to obtain reliable estimation of potential transpiration, especially for such crops where planting system can vary significantly. The need of detailed information on crop traits emphasizing the appealing of remotely sensed data contribution for applications in wide areas. Actual ET estimates obtained using PM-based model always outperform tabled crop coefficient ones, also when an ‘optimal’ (obtained minimizing the error) constant $K_c$ is adopted. The better performance of PM-based approach is partially explained by the capability to intrinsically

account for the daily fluctuations in $K_c$ due to meteorological conditions (*i.e.*, strong or weak wind) as well as for accounting for effective crop characteristics.

By comparing the modeled and observed evapotranspiration fluxes during the irrigation season 2008 (June-October), it was possible to quantify the accuracy of modeled data during the whole irrigation period. In view of the evapotranspiration variability observed in this study, the obtained accuracy seems to be acceptable for irrigation supporting. Analogously, the analysis of actual transpiration dynamic showed a good capability of the model to reproduce system response during both dry days and wet period (after rainfall events). In fact, for a given evaporative demand in the atmosphere, the reduction of crop transpiration by means of stomatal closure seems to be well detected by the model, despite the simplification adopted by the dual-crop coefficient procedure. The overall accuracy in the order of 0.3 mm $d^{-1}$ is generally suitable to support productivity analyses from field-scale to large areas.

The good agreement found in both evapotranspiration and transpiration modeled fluxes with the micrometeorological and sap flow observations, respectively, confirms the capability of the model to correctly separate canopy and soil contributes, thanks to the separation between surface and root zone dynamics in the dual crop coefficient approach. Moreover, the modeled results highlight the negligibility of soil evaporative fluxes during the irrigation phase, as also confirmed by the observations, due to the dripping irrigation system adopted in this site (small wetted area) and nighttime supplies. However, further cross comparisons with approaches that consider the effects of water deficit on the basis of surface temperature observations should improve the understating of the transpiration control phenomena.

Finally, on the basis of the results here discussed, the combination of remote sensing-based potential transpiration assessment with simplified water budget scheme seems a promising and affordable tool to support the extension of such application at field-scale over large irrigated districts and sparse vegetation, where a detailed *in-situ* characterization of crop traits at field scale appears problematic and time and money-consuming. A possible limitation for large area applications is the characterization of minimum stomatal resistance, which may vary from the typical value of 100 m $s^{-1}$ assumed here. While this value performs well for this application, further parameter refinements may be needed for other vegetation types and different locations. It is clear that the information provided by remote sensing data represents a step forward in understanding where improvements in water management can be achieved.

**Acknowledgements.** The authors thank the SIAS (*Servizio Informativo Agrometeorologico Siciliano*) of the *Assessorato Agricoltura e Foreste della Regione Siciliana* for providing the meteorological dataset, the "*Azienda Agricola Rocchetta di Angela Consiglio*" for kindly hosting the experiment. This work was partially funded by the DIFA projects of the Sicilian Regional Government within the *Accordo di Programma Quadro "Società dell'Informazione"*.

## REFERENCES


Abid Karray J, Lhomme JP, Masmoudi MM, Ben Mechlia N (2008) Water balance of the olive tree–annual crop association: A modeling approach. Agric Water Manage 95:575-586.

Allen RG, Jensen ME, Wright JL, Barman RD (1989) Operational estimates of evapotranspiration. Agron J 81:650-662.

Allen RG, Pereira LS, Raes D, Smith M (1998) Crop evapotranspiration. Guideline for computing crop water requirements. FAO irrigation and drainage paper n. 56, Rome, Italy, 326 pp.

Allen RG, Pereira LS (2009) Estimating crop coefficients from fraction of ground cover and height. Irrig Sci 28:17-34.

Allen RG, Pereira LS, Howell TA, Jensen, ME (2011) Evapotranspiration information reporting: I. Factors governing measurement accuracy. Agric Water Manage 98:899-920.

Anderson MC, Neale CMU, Li F, Norman JM, Kustas WP, Jayanthi H, Chavez J (2004) Upscaling ground observations of vegetation water content, canopy height, and leaf area index during SMEX02 using aircraft and Landsat imagery. Remote Sens Environ 92:447-464.

Bausch WC, Neale CMU (1987) Crop coefficients derived from reflected canopy radiation: a concept. Trans Am Soc Agron Eng 30(3):703-709.

Brutsaert W (1982) Evaporation into the atmosphere. Theory, history and applications. Kluwer Academic Publishers, 308 pp.

Cammalleri C, Ciraolo G (2012) State and parameter update in a coupled energy/hydrologic balance model using ensemble Kalman filtering. J Hydrol 416-417:171-181.

Cammalleri C, Anderson MC, Ciraolo G, D'Urso G, Kustas WP, La Loggia G, Minacapilli M (2010) The impact of in-canopy wind profile formulations on heat flux estimation in an open orchard using the remote sensing-based two-source model. Hydrol Earth Syst Sci 14(12):2643-2659.

Cammalleri C, Rallo G, Agnese C, Ciraolo G, Minacapilli M, Provenzano G (2012) Combined use of eddy covariance and sap flow techniques for partition of ET fluxes and water stress assessment in an irrigated olive orchard. Agric Water Manage doi:10.1016/j.agwat.2012.10.003.

Choudhury BJ, Ahmed NU, Idso SB, Reginato RJ, Daughtry CST (1994) Relations between evaporation coefficients and vegetation indices studied by model simulations. Remote Sens Environ 50:1-17.

Clevers JGPW (1989) The application of a weighted infrared-red vegetation index for estimating leaf area index by correcting for soil moisture. Remote Sens Environ 29:25-37.

Crow WT, Kustas WP, Prueger JH (2008) Monitoring root-zone soil moisture through the assimilation of a thermal remote sensing-based soil moisture proxy into a water balance model. Remote Sens Environ 112:1268–1281.

D'Urso G, Menenti M (1995) Mapping crop coefficients in irrigated areas from Landsat TM images. European Symposium on Satellite Remote Sensing II, Europto, Paris; SPIE, Intern. Soc. Optical Engineering, Bellingham (U.S.A.) vol. 2585, 41-47.

Doorenbos J, Pruitt WO (1975) Guidelines for predicting crop water requirements. FAO Irrigation and Drainage Paper n. 24, Rome, Italy, 143 pp.

Er-Raki S, Chehbouni A, Boulet G, Williams DG (2010) Using the dual approach of FAO-56 for partitioning ET into soil and plant components for olive orchards in a semi-arid region. Agric Water Manage 97(11):1769-1778.

Falge E, Reth S, Brüggemann N, Butterbach-Bahl K, Goldberg V, Oltchev A, Schaaf S, Spindler G, Stiller B, Queck R, Köstner B, Bernhofer C (2005) Comparison of surface energy exchange models with eddy flux data in forest and grassland ecosystem of Germany. Ecol Model 188:174-216.

González-Dugo MP, Mateos L (2008) Spectral vegetation indices for benchmarking water productivity of irrigated cotton and sugarbeet crops. Agric Water Manage 95:48-58.

González-Dugo MP, Neale CMU, Mateos L, Kustas WP, Prueger JH, Anderson MC, Li F (2009) A comparison of operational remote sensing-based models for estimating crop evapotranspiration. Agric Forest Meteorol 149:1843-1853.

Granier A (1987) Mesure du flux de sève brute dans le tronc du Douglas par une nouvelle méthode thermique. Ann Forest Sci 44:1-14.

Hartogensis O (2006) Exploring scintillometry in the stable atmospheric surface layer. PhD thesis, Wageningen Universitait, 240 pp.

Heilman JL, Heilman WE, Moore DG (1982) Evaluating the crop coefficient using spectral reflectance. Agron J 74:967-871.

Kalma JD, McVicar TR, McCabe MF (2008) Estimating land surface evaporation: a review of methods using remotely sensed surface temperature data. Surv Geophys 29(4-5):421-469.

Mateos L, González-Dugo MP, Testi L, Villalobos FJ (2012) Monitoring evapotranspiration of irrigated crops using crop coefficients derived from time series of satellite images. I. Method validation. Agric Water Manage http://dx.doi.org/10.1016/j.agwat.2012.11.005.

Minacapilli M, Iovino M, D'Urso G (2008) A distributed agro-hydrological model for irrigation water demand assessment. Agric Water Manage 95(2):123-132.

Minacapilli M, Agnese C, Blanda F, Cammalleri C, Ciraolo G, D'Urso G, Iovino M, Pumo D, Provenzano G, Rallo G (2009) Estimation of actual evapotranspiration of Mediterranean perennial crops by means of remote-sensing based surface energy balance models. Hydrol Earth Syst Sci 13(7):1061-1074.

Monteith JL (1965) Evaporation and environment. In: G.E. Fogg (Ed.), The State and Movement of Water in Living Organisms. XIX Sym Soc Exp Biol 19:205-234.

Penman HL (1956) Estimating evaporation. Trans Am Geophys Union 37:43-46.

Price JC (1990) Information content of soil spectra. Remote Sens Environ 33:113-121.

Pereira LS, Perrier A, Allen RG, Alves I (1999) Evapotranspiration: concepts and future trends. J Irrig Drain Eng ASCE 125(2):45-51.

Rallo G, Provenzano G (2013) Modelling eco-physiological response of table olive trees (Olea europaea L.) to soil water deficit conditions. Agric Water Manage 120:79-88.

Rouse JW, Haas RH, Schell JA, Deering DW (1973) Monitoring vegetation systems in the Great Plains with ERTS. Third ERTS Symposium, NASA SP-351 I, 309-317.

Santos C, Lorite, IJ, Allen RG, Tasumi M (2012) Aerodynamic Parameterization of the Satellite-Based Energy Balance (METRIC) Model for ET Estimation in Rainfed Olive Orchards of Andalusia, Spain. Water Resour Manage 26(11):3267-3283.

Sellers PJ, Heiser MD, Hall FG (1992) Relations between surface conductance and spectral vegetation indices at intermediate (100 $m^2$ to 15 $km^2$) length scales. J Geophys Res 97(D17):19033–19059.

Slater P, Biggar S, Thome K, Gellman D, Spyak P (1996) Vicarious radiometric calibrations of EOS sensors. J Atmos Ocean Tech 13:349-359.

Thiermann V, Grassl H (1992) The measurement of turbulent surface-layer fluxes by use of bichromatic scintillation. Boundary Layer Meteorol 58:367-389.

van Diepen CA, Rappoldt C, Wolf J, van Keulen H (1988) Crop growth simulation model WOFOST. Doc v4.1. Centre for World Food Studies, Wageningen, The Netherlands.

Wright JL (1982) New evapotranspiration crop coefficients. J Irrig Drain Div ASCE 108:57-74.

## TABLES

**Table 1.** Airborne images acquisition scheduling and mean overpass times.

| Date (dd/mm/yyyy) | DOY | Time (local*) |
|---|---|---|
| 11/06/2008 | 163 | 13:30 |
| 03/07/2008 | 185 | 11:00 |
| 22/07/2008 | 204 | 11:30 |
| 22/08/2008 | 235 | 12:00 |
| 03/09/2008 | 247 | 11:30 |
| 10/10/2008 | 284 | 11:00 |
| 21/10/2008 | 295 | 11:30 |

* local time = UTC+2

**Table 2.** Soil parameters used for the FAO-56 hydrological model simulation.

| Parameter | Description | Value |
|---|---|---|
| REW (mm) | Readily evaporable water | 10 |
| TEW (mm) | Total evaporable water | 25 |
| $\theta_{wp}$ ($m^3$ $m^{-3}$) | Water content at wilting point | 0.09 |
| $\theta_{fc}$ ($m^3$ $m^{-3}$) | Water content at field capacity | 0.32 |
| $f_w$ | Fraction of soil surface wetted by irrigation | 0.2 |
| $f_{ew}$ | Fraction of soil exposed and wetted during irrigation | 0.1 |
| $Z_e$ (m) | Surface layer thickness | 0.10 |
| $Z_r$ (m) | Root zone thickness | 0.90 |

## LIST OF FIGURES

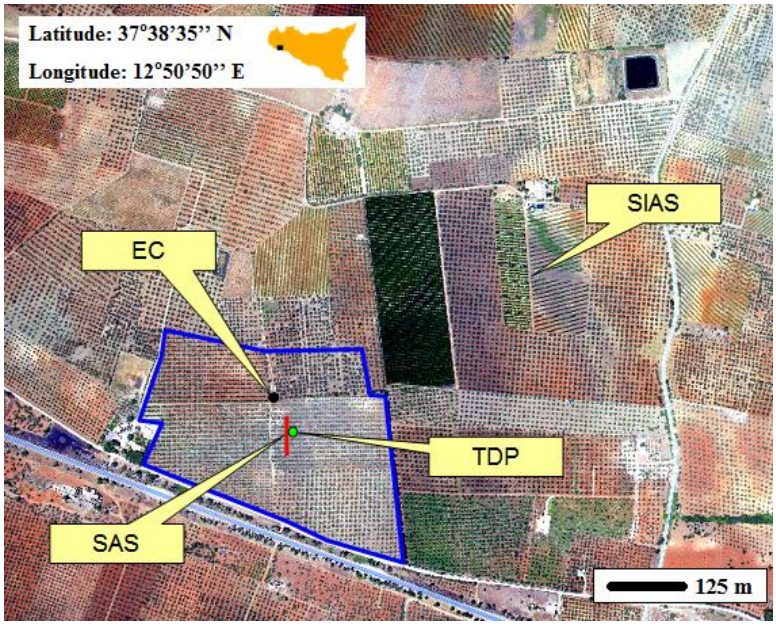


**Fig. 1.** Orthophoto of the study area with localization of the experimental olive field demarcated by blue line. Location of SIAS weather station is reported, as well as eddy covariance (EC), scintillometer (SAS) and sap flow (TDP) installations adopted to monitor surface fluxes.

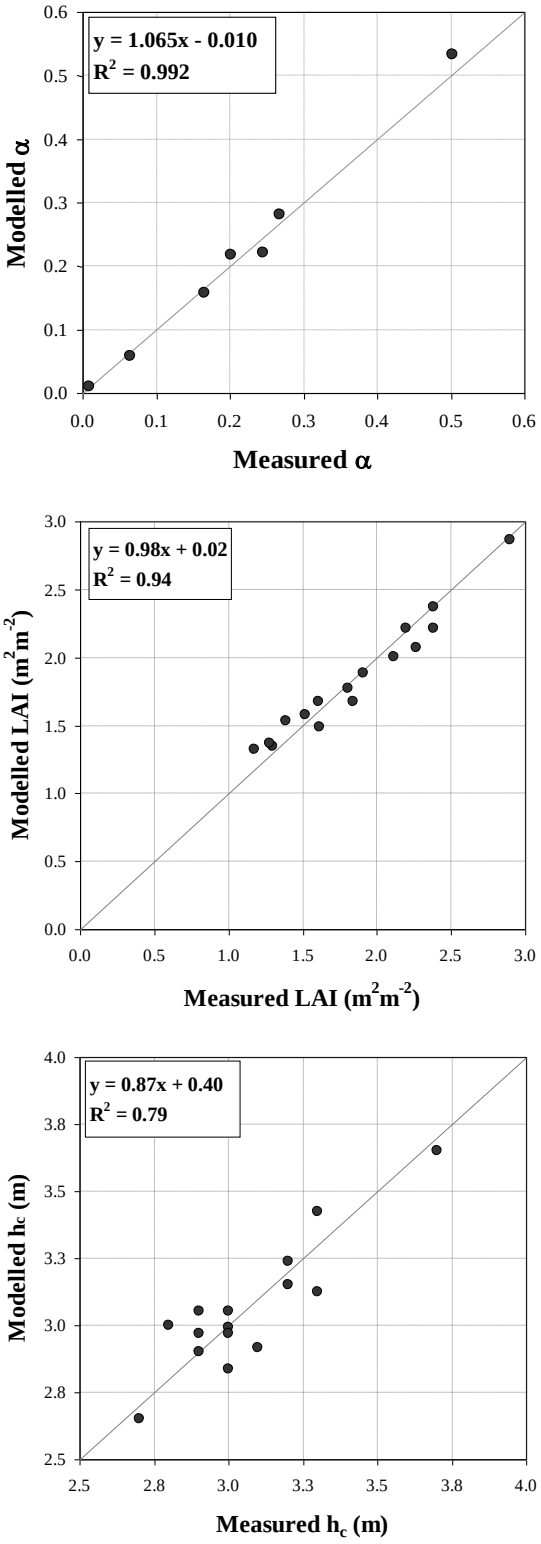


**Fig. 2.** Example of calibration accuracy for albedo (upper panel), LAI (middle panel) and crop height (lower panel) maps for the first acquisition (DOY 163).

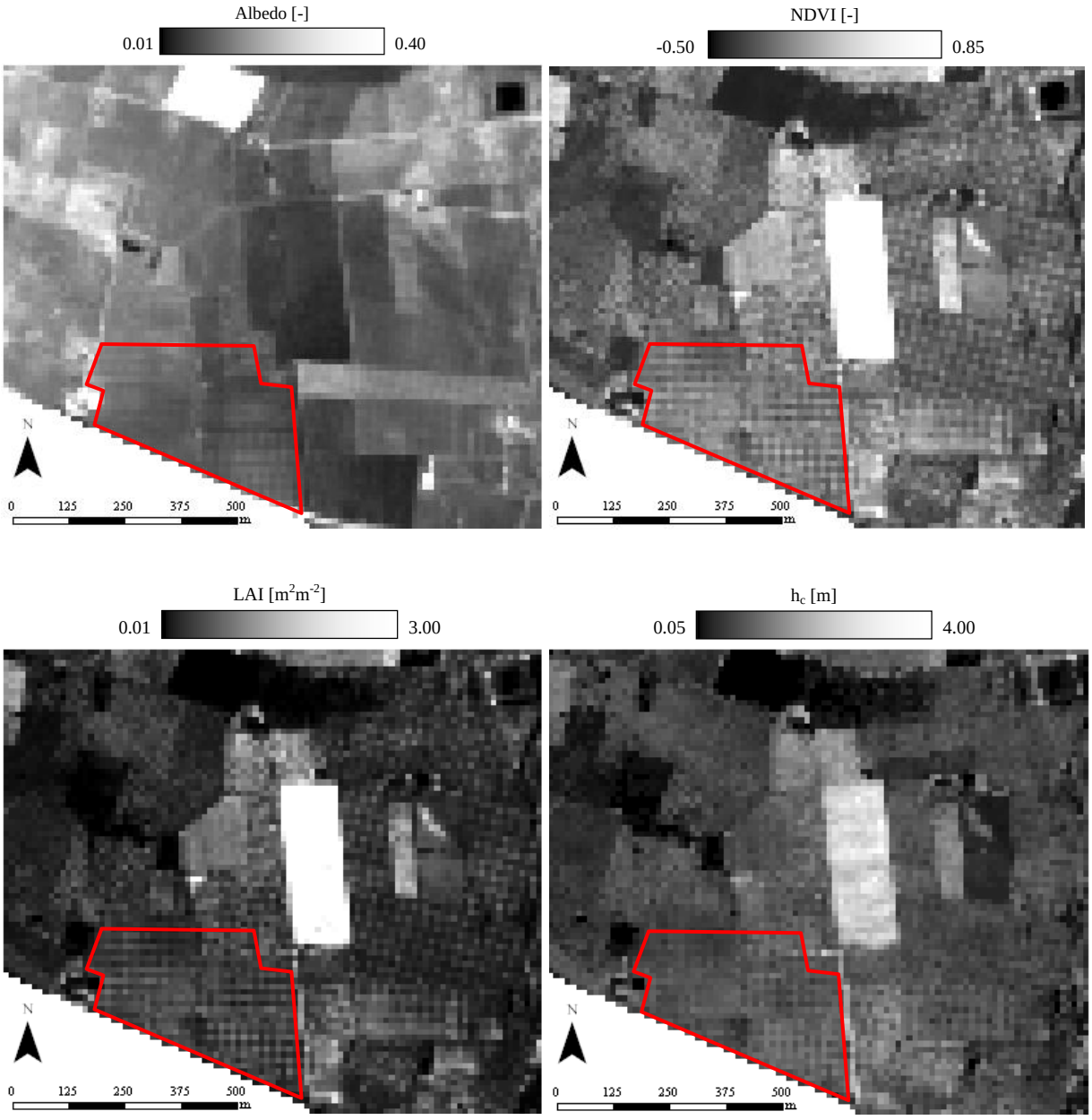


**Fig. 3.** Spatial distribution of albedo (upper left panel), NDVI (upper right panel), LAI (lower left panel) and $h_c$ (lower right panel) for the DOY 185, at a spatial resolution of 12 m. Red line demarks the experimental olive field.

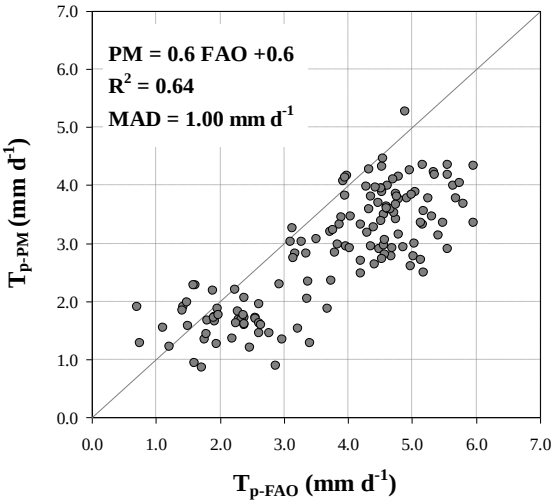


**Fig. 4.** Scatterplot between $T_p$ values retrieved by the PM formulation and the FAO-56 one.

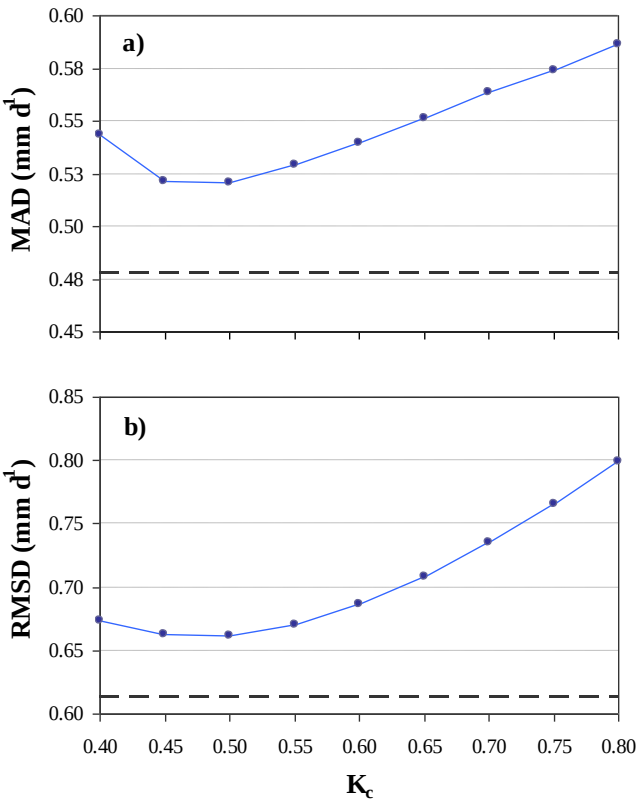


**Fig. 5.** Analysis of mean absolute difference (MAD, panel a) and root mean square difference (RMSD, panel b) as a function of $K_c$. Dotted lines represent the values obtained for PM-based simulation.

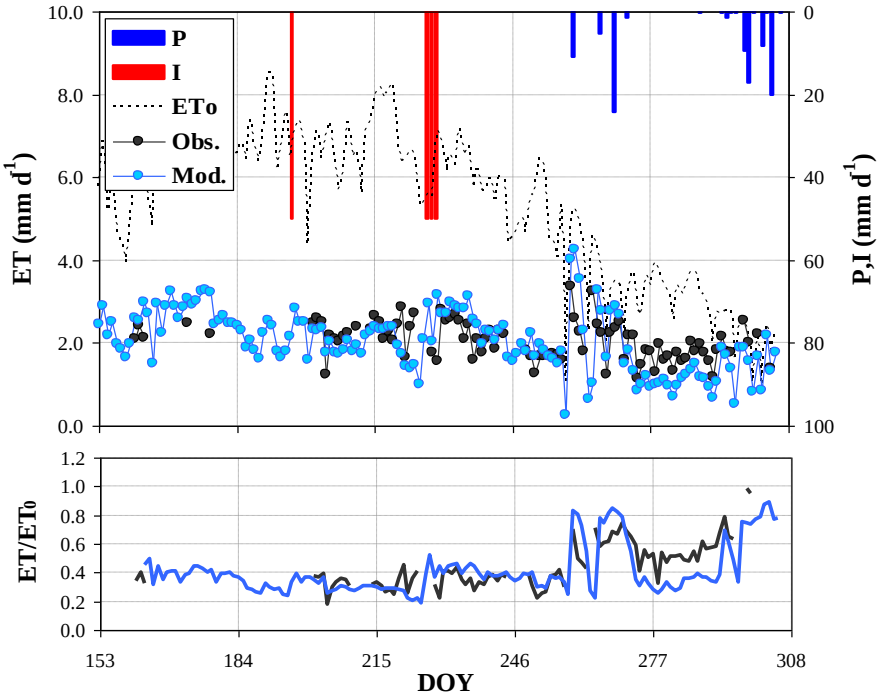


**Fig. 6.** Temporal dynamic of daily *ET*. Main panel: Obs. values (black dots) correspond to the observations made by micro-meteorological systems, Mod. values (cyan dots) are the ones modeled by means of dual-$K_c$ scheme and PM approach, and ETo values (dotted line) are the $ET_0$ derived applying the FAO-56 formulation using the locally observed weather data (left y-axis). Bars represent the rainfall (red) and irrigation (blue) inputs (right y-axis). Secondary panel: Obs. and Mod. values are normalized through reference ET.

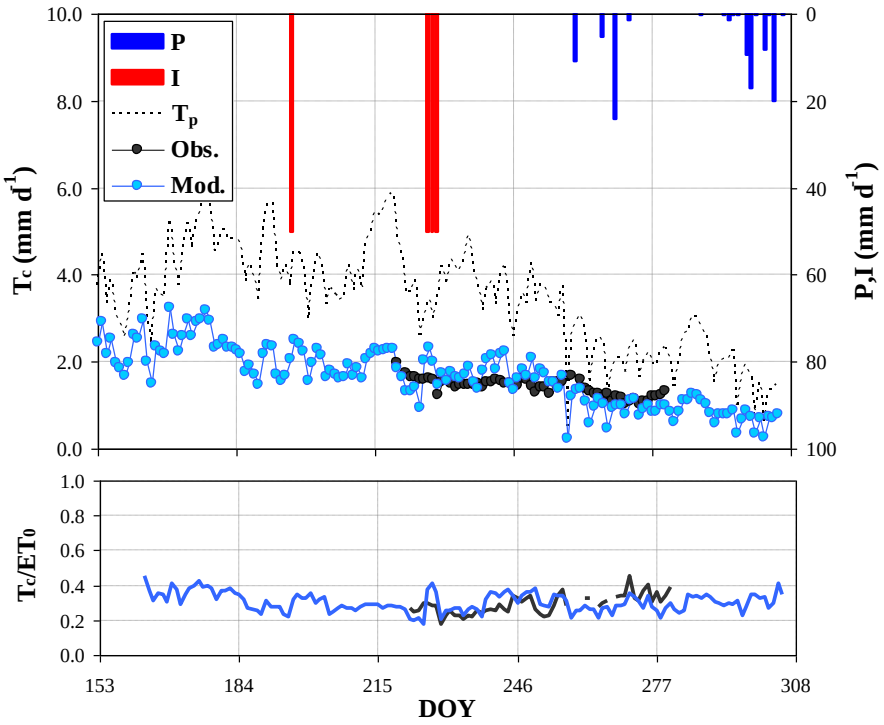


**Fig. 7.** Temporal trend of daily $T_c$. Main panel: Obs. values (black dots) correspond to the observations made by sap flow installations, Mod. values (cyan dots) are the ones modeled by means of dual-$K_c$ scheme and PM approach, and $T_p$ values (dotted line) are the crop potential ET computed with the PM formulation using the remotely observed data (left y-axis). Histograms represent the rainfall (red) and irrigation (blue) inputs (right y-axis). Secondary panel: Obs. and Mod. values are normalized through reference ET.

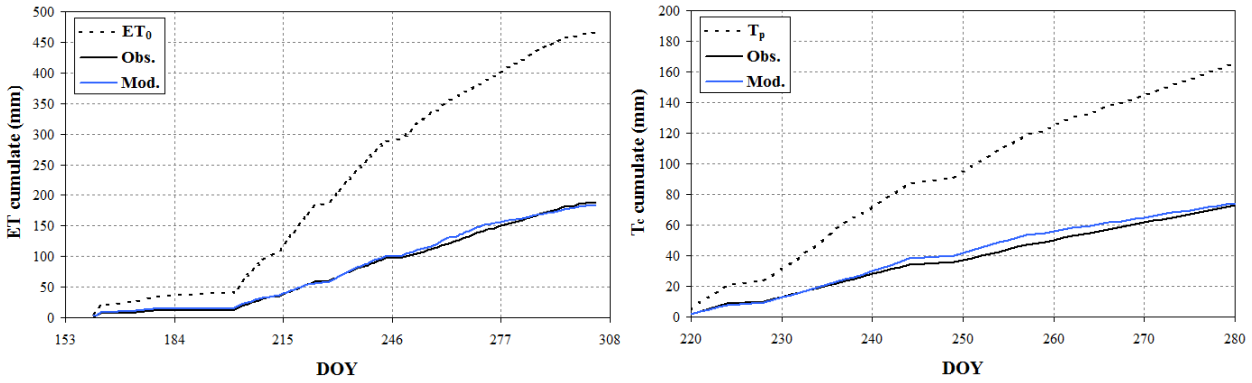


**Fig. 8.** Cumulative observed (black line) and modeled (cyan line) *ET*, left panel, and $T_c$, right panel. Dotted line represents the cumulated $ET_0$ and $T_p$, respectively. The x-axis of each panel is tailored to the available range of dates of the corresponding observed variable.